

Cite this: DOI: 00.0000/xxxxxxxxxx

# Dynamic control of self-assembly of quasicrystalline structures through reinforcement learning

Uyen Tu Lieu,<sup>\*†a,b</sup> Natsuhiko Yoshinaga<sup>†a,b</sup>Received Date  
Accepted Date

DOI: 00.0000/xxxxxxxxxx

We propose reinforcement learning to control the dynamical self-assembly of the dodecagonal quasicrystal (DDQC) from patchy particles. The patchy particles have anisotropic interactions with other particles and form DDQC. However, their structures at steady states are significantly influenced by the kinetic pathways of their structural formation. We estimate the best policy of temperature control trained by the Q-learning method and demonstrate that we can generate DDQC with few defects using the estimated policy. The temperature schedule obtained by reinforcement learning can reproduce the desired structure more efficiently than the conventional pre-fixed temperature schedule, such as annealing. To clarify the success of the learning, we also analyse a simple model describing the kinetics of structural changes through the motion in a triple-well potential. We have found that reinforcement learning autonomously discovers the critical temperature at which structural fluctuations enhance the chance of forming a globally stable state. The estimated policy guides the system toward the critical temperature to assist the formation of DDQC.

## 1 Introduction

Nano- and colloidal self-assembly is promising due to its high potential in creating complex structures with emergent photonic,<sup>1,2</sup> magnetic,<sup>3</sup> and electronic<sup>4</sup> properties. To make various self-assembly structures, several methods have been proposed, such as patchy particles,<sup>5–7</sup> non-spherical particles,<sup>8</sup> and particles with non-monotonic interactions.<sup>9</sup> Among those, the patchy particle, which has anisotropic interactions, is a good candidate due to its high flexibility in designing the interactions and the capability to form complex structures.<sup>6,10</sup> In fact, complex structures, such as diamonds and quasicrystals, are reproduced by using patchy particles. Still, designing a desired structure remains a formidable task and relies on trial and error.

Recently, there has been growing interest in the inverse design of desired self-assembly structures. In the conventional forward-type approach, we start from a given model with a specific type of interaction between particles and tune its parameters to analyse the obtained structure. In contrast, the inverse design estimates the model from the desired structure. This approach has been successfully applied to several complex structures, such as quasicrystals.<sup>11–14</sup> However, so far, the methods of the inverse design rely on static control, such as optimisation of parameters in the potential interactions, and do not take into account the kinetic process

of self-assemblies. It is well known that the steady-state structure is largely affected by dynamic control, such as the change in temperature and external mechanical forces.

To design self-assembly structures by dynamic control, we need to access their kinetic pathways, which are unknown from the static interactions. Systems may often have many metastable states even under the same parameters. As a result, once the structure gets trapped in the metastable state at a low temperature, the system hardly escapes from it to reach the global energy minimum. Let us take an example of the two-dimensional dodecagonal quasicrystal (DDQC) self-assembled from five-fold symmetrical patchy particles. The DDQC can be attained by linearly slowly decreasing temperature in the system (annealing).<sup>7</sup> The obtained structures are not always ideal as the assemblies may have defects. This is particularly the case when the speed of temperature change is too fast. In this case, the DDQC structure no longer appears. In a Monte Carlo simulation of five-patch patchy particles,<sup>15</sup> the temperature is quickly cooled down to zero, and then subsequently it is fixed at a specific value. This two-step temperature protocol was developed empirically. The challenge is to find a method that can learn and find suitable temperature settings to facilitate DDQC with few defects, under no or few prior knowledge. In this study, we will show that reinforcement learning is useful for this purpose.

Reinforcement learning (RL) is a branch of machine learning that aims to learn an optimal policy and protocol to interact with the environment through experience. From the viewpoint of physical science, RL can estimate an external force or parameter change as a function of the state of the system. Therefore,

<sup>a</sup> Advanced Institute for Materials Research (AIMR), Tohoku University, Katahira 2-1-1, Sendai 980-8577, Japan. E-mail: uyen.lieu.tu.d3@tohoku.ac.jp

<sup>b</sup> Mathematics for Advanced Materials-OIL, AIST, Katahira 2-1-1, Sendai 980-8577, Japan. Tel: +81-(0)22-237-8017; E-mail: yoshinaga@tohoku.ac.jp

† These authors contributed equally to this work.

RL shares many aspects with adaptive optimal control theory.<sup>16</sup> RL can be versatily applied in strategy games,<sup>17,18</sup> robotics,<sup>19</sup> and physics problems. Applying RL in dynamical physical problems, such as fluid mechanics<sup>20,21</sup> and navigation of a single self-propelled particle,<sup>22</sup> is promising because of its capability of finding the best control policy by iterating (experiencing) the dynamical processes without any prior knowledge. RL has been applied in optimising the best operational parameters for a system,<sup>23,24</sup> or tuning the operational parameter during a dynamical process.<sup>22</sup> Few studies have focused on many-body particles and their collective behaviours of active matter systems<sup>25–27</sup> or self-assemblies.<sup>24,28</sup> In Ref.<sup>24</sup>, the Q-learning algorithm<sup>29</sup> is used to remove grain boundaries from a crystalline cluster of colloids.

In this work, we propose a method using RL to optimise the assembly of the two-dimensional dodecagonal quasicrystalline structure from five-fold symmetric patchy particles. We aim to find the best temperature schedule for creating the DDQC, and explain how RL works in this system. The paper is organised as follows: In Sec. 2, we explain our system and the simulations of the self-assembly, the basics of RL and the Q-learning approach, and the setting of the assembly problem into Q-learning. In Sec.3, we show how the policy is estimated during training, and how the estimated policy works during tests to evaluate its optimality. The capability of RL is addressed in terms of the advantage over the conventional temperature schedule and the scalability. In Sec. 4, we discuss the issues on the training cost and the discreteness of states in Q-learning, and then conclude.

## 2 Methods

### 2.1 Self-assembly of patchy particles through Brownian Dynamics simulations

Our system consists of  $N$  patchy particles. Each particle stochastically moves and rotates following the equations (1) and (2) under the temperature  $T$  at time  $t$  (see Fig. 1(b)). The patchy particle has anisotropic interactions with other particles. Depending on the anisotropy, the particles may form an ordered self-assembled structure. Because the thermal fluctuation of the particles is dependent on the temperature, the self-assembled structure varies as the temperature changes.

The Brownian dynamics (BD) simulation is employed to simulate the assembly of five-fold-symmetric patchy particles.<sup>7,13</sup> The patchiness on the spherical particle is described by the spherical harmonic of  $Y_{55}$ . There are 5 positive patches and 5 negative patches arranged alternatively around the particle's equator (see Fig. 1(b)). We set that the same sign patches are attractive while opposite patches are repulsive. The particles are confined to a flat plane, meaning that the particles can translate on the plane while they can rotate freely in three dimensions. In the Brownian dynamics, the position  $\mathbf{r}$  and orientation  $\mathbf{\Omega}$  of the particle are updated according to the equations

$$\mathbf{r}(t + \Delta t) = \mathbf{r}(t) + \frac{D^T}{k_B T} \mathbf{F}(t) \Delta t + \delta \mathbf{r}, \quad (1)$$

$$\mathbf{\Omega}(t + \Delta t) = \mathbf{\Omega}(t) + \frac{D^R}{k_B T} \mathbf{T}(t) \Delta t + \delta \mathbf{\Omega}, \quad (2)$$

where  $D^T, D^R$  are the translational and rotational diffusion coefficients, respectively,  $k_B$  is the Boltzmann constant,  $\mathbf{F}$  and  $\mathbf{T}$  are the force and torque, the Gaussian noise terms  $\delta \mathbf{r}$  and  $\delta \mathbf{\Omega}$  are with zero mean and satisfying  $\langle \delta \mathbf{r} \delta \mathbf{r}^T \rangle = 2D^T \Delta t$  and  $\langle \delta \mathbf{\Omega} \delta \mathbf{\Omega}^T \rangle = 2D^R \Delta t$ , respectively. The characteristic length, energy, time, and temperature for the nondimensionalisation are the particle radius  $a$ , the potential well-depth  $\varepsilon_V$ , the Brownian diffusion time  $\tau_B = a^2/D^T$ , and  $\varepsilon_V/k_B$ , respectively.

The interaction potential of a pair of particles  $i$  and  $j$  is  $V_{ij} = V_{\text{WCA}}(r_{ij}) + V_{\text{M}}(r_{ij})\Xi(\mathbf{\Omega}_{ij})$ . The isotropic Week-Chandler-Anderson term  $V_{\text{WCA}}$  prevents the overlapping of particles. The interaction of the patchiness is given by the Morse potential  $V_{\text{M}}$  and the mutual orientation dependent term  $\Xi(\mathbf{\Omega}_{ij})$ .

$$V_{\text{WCA}} = \begin{cases} 4\varepsilon_V \left[ \left( \frac{2a}{r} \right)^{12} - \left( \frac{2a}{r} \right)^6 + \frac{1}{4} \right], & r \leq 2a\sqrt[6]{2} \\ 0, & r > 2a\sqrt[6]{2} \end{cases} \quad (3)$$

$$V_{\text{M}} = \varepsilon_V M_d \left\{ \left[ 1 - e \left( -\frac{r - r_{\text{eq}}}{M_r} \right) \right]^2 - 1 \right\}, \quad (4)$$

where  $r$  is the center-particle distance;  $\varepsilon_V$  is the Morse potential equilibrium position, depth and range are respectively  $r_{\text{eq}} = 1.878a$ ,  $M_d = 2.294a$ , and  $M_r = a$ .<sup>30</sup>

The orientation of particle  $i$  is determined by the orthogonal local bases  $\hat{\mathbf{n}}_m^{(i)}$ ,  $m = 1, 2, 3$ . Let  $\hat{\mathbf{r}}$  be the unit distance vector of particle  $i$  and  $j$ . The interaction of a pair of particle  $Y_{lm}$  is  $\Xi_{lm} \propto \{\hat{\mathbf{n}}_0^{l-m} \hat{\mathbf{n}}_+^m\}_{(i)} \odot \{\hat{\mathbf{r}}^{2l}\} \odot \{\hat{\mathbf{n}}_0^{l-m} \hat{\mathbf{n}}_+^m\}_{(j)}$ , where  $\hat{\mathbf{n}}_0 = \hat{\mathbf{n}}_3$ ,  $\hat{\mathbf{n}}_+ = \frac{1}{\sqrt{2}}(\hat{\mathbf{n}}_1 + i\hat{\mathbf{n}}_2)$ , and the  $\{\}$  indicates the irreducible tensor. For a pair of  $Y_{55}$  particles  $\Xi_{55} \propto \{\hat{\mathbf{n}}_+^5\}_{(i)} \odot \{\hat{\mathbf{r}}^{10}\} \odot \{\hat{\mathbf{n}}_+^5\}_{(j)}$ , and  $\Xi$  is normalised to be in the range of  $[-1, 1]$ .

### 2.2 Reinforcement Learning and Q-learning

The basic ingredients of Reinforcement learning (RL) include an agent, an environment, and reward signals (Fig. 1). The agent observes the states  $s$  of the environment and learns optimal actions  $a$  through a policy  $\pi$  that maximises the cumulative future rewards  $R$ .<sup>31</sup> The future reward is the sum of the instantaneous reward  $r_i$  at each step  $i$

$$R = \sum_i \gamma r_i, \quad (5)$$

with the discount factor  $\gamma$ . Formally, RL is expressed by a tuple of  $\{\mathcal{S}, \mathcal{A}, \mathcal{P}, g, \pi\}$  where  $\mathcal{S}$  is a state space,  $\mathcal{A}$  is an action space,  $\mathcal{P}$  is a Markov transition process of the environment describing its time evolution,  $g$  is the (instantaneous) reward function, and  $\pi$  is a policy (Fig. 1(a)). The transition process  $P(s_{t+1}|s_t, a_t) \in \mathcal{P}$  maps the current state  $s_t \in \mathcal{S}$  to the next state  $s_{t+1}$  under the action  $a_t \in \mathcal{A}$ . The process is supplemented by the initial probability of the states  $P(s_0)$ . The reward measures whether the current state is good or bad. The reward function gives some numbers from the current state and action as  $r_t = g(s_t, a_t)$ . In this work, we assume the reward function is dependent only on the state, that is,  $r_t = g(s_t)$ . In general, the policy is a conditional probability  $\pi(a|s)$  of taking the action under a given state. In this work, we assume the deterministic policy  $a(s)$ , namely, the action is the function of the state.

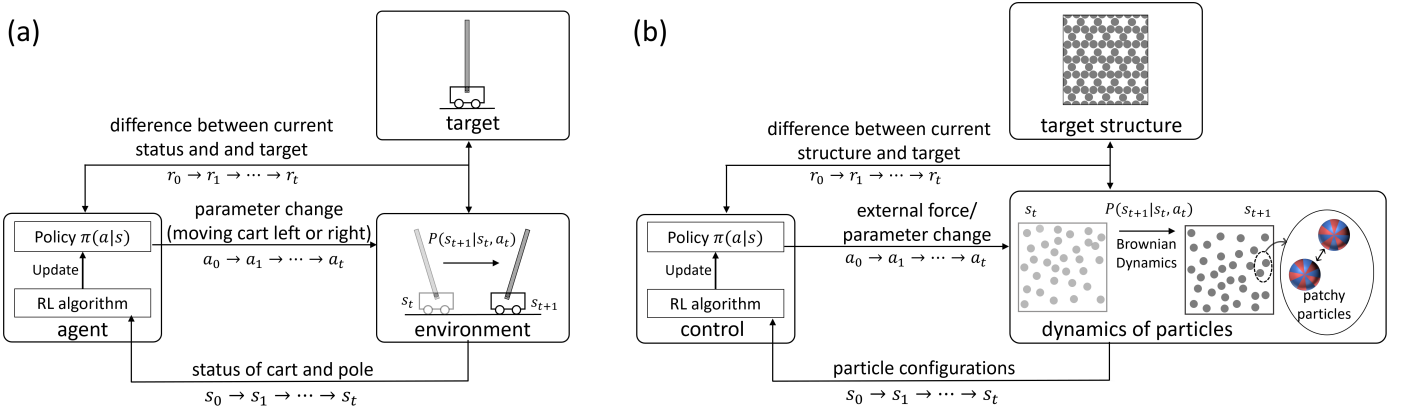


Fig. 1 Schematic of reinforcement learning for (a) cart-pole problem and (b) dynamic self-assembly. The agent observes the state  $s$  from the environment, and decides to take an action  $a$  based on the policy  $\pi$ . The agent learns the policy  $\pi$  by a training process to optimise the rewards  $r$ . In this study, the environment is the particle configuration under a given temperature. The observed states are the ratio of sigma particle  $\sigma$  and temperature  $T$ . The action is to decrease, maintain, or increase the current temperature.

A physical interpretation of RL is to estimate the best dynamic control strategy to get a desired structure or physical property (see Fig. 1(b)). The physical system of variables  $s_t$  yields the dynamics expressed by the Markov process  $\mathcal{P}(s_{t+1}|s_t, a_t)$  under an external force and/or parameter change in the model expressed by  $a_t$ . At each time, we can compare the current state  $s_t$  and the target state  $s^*$ . The distance between them is an instantaneous reward. The goal of RL is to estimate the best policy from which we choose the action  $a$  as a function of the current state  $s$ .

In the context of self-assemblies, RL aims to control the external force or the parameters so that the desired structure is organised from a random particle configuration. In this study, we control temperature; our action is whether temperature increases, decreases, or stays at the current value. The environment is the configuration of the particles at certain conditions, such as temperature and density. In principle, the dimension of the state space is huge. It may be all the degrees of freedom of the particles, their positions and orientations. Nevertheless, our purpose is to make the desired structure, which is the DDQC structure. Therefore, we use statistical quantities (or feature values) to characterise the particle configurations. This is the number of  $\sigma$  particles, denoted as  $N_\sigma$ ; we will discuss this issue in detail in Sec. 2.3. We consider two observed states from the environment: the temperature  $T$  and the ratio of  $\sigma$  particles of the DDQC, which is extracted from the particle configuration, to the total particles. We denote the ratio by  $\sigma = N_\sigma/N$ . From the observed states, we take an action  $a$  updating the current temperature to the next one. We also get a reward  $r_t$  from the measured state. From the reward, the next action is decided at each step and the procedure continues to update all different states. Within each step, the configuration of particles is updated by BD simulations.

There are many RL algorithms to train the agent. Q-learning is a popular algorithm for learning optimal policies in Markov decision processes.<sup>32</sup> It is a model-free, value-based algorithm that uses the concept of Q-values (Quality value) to guide the agent's decision-making process. Q-value, denoted as  $Q(s, a)$ , is the cumulative reward obtained by taking action  $a$  on the current state

$s$  and then following the optimal policy. The simplest Q-learning uses a Q-table in which Q-values are updated at each point in discretised action and state spaces. The size of Q-table depends on the number of elements of the state spaces and action spaces. For example, consider a system with two state spaces discretised into  $m$  and  $n$  elements, and an action space with  $l$  elements. In this case, the corresponding Q-table is a three-dimensional array with dimensions  $m \times n \times l$ . This array represents the whole state-action space, in which the agent (we) can store and update Q-values for all possible combinations of states and actions. The policy is then extracted from the Q-value of each state-action pair  $Q(s, a)$ . In general, the algorithm involves many epochs (or episodes). The Q-table is initialised at first. For each epoch, the states are also initialised, then for each step in the epoch, we perform the following algorithms:

- Observe a current state  $s_t \in \mathcal{S}$ .
- Select and perform an action  $a_t \in \mathcal{A}$  based on the policy from  $Q(s, a)$ .
- Observe the subsequent state  $s_{t+1}$ .
- Receive an immediate reward  $r_{t+1}$ .
- Update iteratively the Q-function by

$$Q(s_t, a_t) = Q(s_t, a_t) + \alpha[r_{t+1} + \gamma \max_a Q(s_{t+1}, a) - Q(s_t, a_t)] \quad (6)$$

where learning rate  $\alpha$  is a hyperparameter  $0 \leq \alpha \leq 1$  that reflects the magnitude of the change to  $Q(s_t, a_t)$  and the extent that the new information overrides the old information. If  $\alpha = 0$ , no update at all; if  $\alpha = 1$ , then completely new information is updated in  $Q$ . The discount factor  $\gamma$  is associated with future uncertainty or the importance of the future rewards ( $0 \leq \gamma \leq 1$ ).

In RL, it is important to consider the balance between exploitation and exploration. If we just follow the current (non-optimal) policy, it is unlikely to find potentially more desired states. On the other hand, if our search is merely random, it takes a significant amount of time to find them. In Q-learning, exploitation involves

selecting the action that is believed to be optimal, i.e. maximum Q-value, while exploration involves selecting the action that does not need to be optimal within the current knowledge. To balance these strategies, the  $\epsilon$ -greedy method is used. In the  $\epsilon$ -greedy method, a random action at each time step is selected with a fixed probability  $0 \leq \epsilon \leq 1$  instead of the optimal action with respect to the Q-table.

$$\pi(s) = \begin{cases} \text{random action } a \in \mathcal{A}, & \text{if } \xi < \epsilon \\ \arg \max_{a \in \mathcal{A}} Q(s, a), & \text{otherwise,} \end{cases} \quad (7)$$

where  $0 \leq \xi \leq 1$  is a uniform random number at each step.

### 2.3 Characterisation of DDQC structures

In two-dimensional DDQC, one method to characterise DDQC structure is to determine each particle according to its nearest neighbour structure<sup>7,15</sup> (Fig. 2). Given the particle positions, the sigma, hexagonal Z, and H local structures are estimated. A DDQC structure usually contains a few Z dispersed in many sigma and a few H particles. In our simulations, the value of  $\sigma = N_\sigma / N$  ( $N_\sigma$  is the number of sigma particles) is observable and it can express the quality of a DDQC; therefore we choose  $\sigma$  as one of the states of the RL ( $0 \leq \sigma \leq 1$ ).

Ideally, the ratio of the sigma particles to the total particle is expected to reach  $0.86 \leq \sigma \leq 0.93$ . However, at finite temperatures, defects can always appear in the self-assembled structures. We consider that structures with  $\sigma \gtrsim 0.7$  are global minimum DDQCs with a few defects. The quality of DDQC for that value of  $\sigma$  is demonstrated in its Fourier transformation image showing distinguishable 12-fold symmetry spots from the background. When  $0.5 \leq \sigma \leq 0.7$ , we refer the structures to be metastable states with many defects.

Another state is the temperature  $T$ . The range of the temperature is chosen as  $0.2 \leq T \leq 1.3$  so that the particle interaction dominates the noise at  $T_{min}$  and the noise dominates the interaction at  $T_{max}$ .

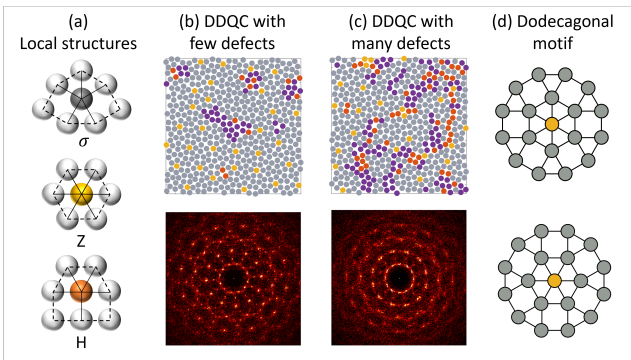


Fig. 2 Characterisation of DDQCs. (a) Demonstration of local structures. (b-c) Examples of DDQC with few and many defects, and the correspondent Fourier transformations. The defect points are marked purple. The fraction of sigma in (b-c) are 0.84 and 0.67, respectively. (d) Dodecagonal motif made from one Z particle centred in 18  $\sigma$  particles.

### 2.4 Reinforcement learning for dynamic self-assembly

The schematic for Q-learning in this study is given in Fig. 3. Initially, Q-table is set to zero for all  $a$  and  $s$ . The RL includes  $N_e$  epochs or episodes in which the  $\epsilon$ -greedy method is applied. In each epoch, the initial state, i.e. the initial particle configuration and the initial temperature ( $\sigma_0, T_0$ ) are assigned. Next, the action  $a_0$  (either decrease, maintain, or increase  $T$ ) for the temperature is decided based on the current policy and the  $\epsilon$ -greedy strategy, resulting in the new temperature  $T_1$ . The Brownian dynamics simulation for the current particle configuration at  $T_1$  is conducted. Details of the Brownian dynamics simulation can be found in section 2.1. The new particle configuration is obtained after a predetermined time  $t = N_{BD}\Delta t$ . Then one can determine the state  $\sigma_1$ , the reward  $r_1$ , and eventually update the Q-value  $Q(\sigma_0, T_0, a_0)$ . This concludes the Q-learning of the first step. The next step can be conducted analogically from the current state ( $\sigma_1, T_1$ ). The Q-table is updated at every action step, every epoch, until the training process ends.

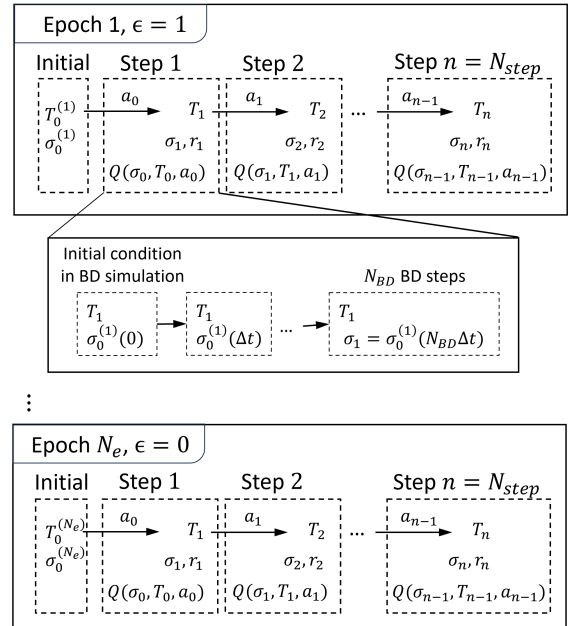


Fig. 3 Schematic of Q-learning at each epoch with  $\epsilon$ -greedy method. The action  $a$  is chosen based on the current policy  $\pi$  and  $\epsilon$ . Q is updated according to eq. (6). Brownian dynamics (BD) simulation is conducted for every step in  $N_{step}$  of each epoch.

From the trained Q-table, we can estimate the policy on controlling the temperature with respect to the current state. In order to evaluate the estimated policy, 20 independent tests are conducted. Each test starts with an assigned initial particle configuration and temperature (initial states), followed by consecutive steps of deciding the next action based on the estimated policy, observing the new states, and so on. Otherwise stated, we set the parameters the same as the parameters used during training, except that  $\epsilon = 0$  is fixed in every test.

Table 1 shows the parameters of a training set. The two observed states are the ratio of sigma particle  $\sigma$  and the temperature  $T$ . Initially, the configuration of the particle is random (corresponding to  $\sigma_0 < 0.1$ ) and  $T_0$  values are chosen randomly in the



investigated range. While the fraction of sigma never reaches out of the range  $[0, 1]$ , the temperature  $T_{k+1}$  after the action  $a_k$  may exceed the investigated range. In this case, the updating is carried out as usual except that we treat  $T_{k+1} = T_k$ . The policy after training is used for the test at the same conditions as training (except  $\epsilon$ ). We use different training sets; the condition of each set is given in Table 2. The main difference is the choice of initial temperature in each epoch.

Parameter	Value
States of sigma fraction, $\sigma$	$[0, 1]$ , intervals of 0.1
States of temperature, $T$	$[0.2, 1.3]$ , intervals of 0.1
Actions on the temperature, $a$	$\{-0.05, 0, 0.05\}$
Number of epochs, $N_e$	101
$\epsilon$	linearly decrease in each epoch from 1 to 0
Initial temperature at each epoch, $T_0$	random
Initial structure at each epoch, $\sigma_0$	random ( $\sigma_0 < 0.1$ )
Number of action steps in each epoch, $N_{step}$	200
Number of BD steps in each BD simulation, $N_{BD}$	100,000 steps equivalent to $t = 10$
Target, $\sigma^*$	0.9
Rewards, $r$	$-(\sigma - \sigma^*)^2$
Learning rate, $\alpha$	0.7
Discount factor, $\gamma$	0.9
Number of particles, $N$	256
Area fraction	0.75

Table 1 Parameters for the training data.

Parameters	All $T_0$ set	Low $T_0$ set	High $T_0$ set	completely off-policy
$\sigma^*$	0.9	0.9	0.9	0.81
$T_0$	$[0.2, 1.3]$	0.22	1.22	1.22
$N_{epoch}$	10, 20, 40, 101	10, 20, 40	10, 20, 40	1
$\epsilon$	decrease	decrease	decrease	1
$N_{step}$	200	200	200	4000

Table 2 Setting of other training sets

## 2.5 Q-learning for triple-well potential model

Similar to the DDQC, we apply Q-learning for a model consisting of two state variables  $x$  and  $T$ . The states follow the dynamics described by the following Langevin equations

$$x(t+dt) = x(t) - \partial_x U(x, T)dt + \xi_x \quad (8)$$

$$T(t+dt) = T(t) + a + \xi_T. \quad (9)$$

The state  $x$  moves in the  $T$ -dependent potential  $U(x, T)$ , whereas  $T$  evolves through the action  $a$  with noise. The functional form of the potential is shown in Fig. 8. The fluctuation of  $x$  is illustrated by the noise term  $\xi_x$ . The relation of  $x$  and  $T$  is described by a triple-well potential  $U(x, T) = -\frac{1}{\tau} \sum_{i=1}^3 \mathcal{N}_i(x; \mu_i, \sigma_{pi}) h_i(T)$  where  $\mathcal{N}_i(x; \mu_i, \sigma_{pi})$  is the Gaussian distribution with mean  $\mu_i$  and standard deviation  $\sigma_{pi}$ ,  $h_i(T)$  is a temperature dependent function. By designing  $\mathcal{N}_i(x; \mu_i, \sigma_{pi})$  and  $h_i(T)$ , the position and the depth of the well can be controlled. The parameter of each well is  $\mu_1 = 0.16$ ,  $\sigma_{p1} = 0.2$ ,  $h_1(T) = T^2$ ,  $\mu_2 = 0.55$ ,  $\sigma_{p2} = 0.11$ ,  $h_2(T) =$

$(1.5 - T)^4$ ,  $\mu_3 = 0.88$ ,  $\sigma_{p3} = 0.11$ ,  $h_3(T) = 1.8(1.4 - T)^4$ . With the choice of parameters, our triple-well potential has minima at  $x = \mu_1, \mu_2, \mu_3$ . The potential minimum at  $x = \mu_1$  is shallow, whereas the potential minima at  $x = \mu_2, \mu_3$  are deeper. The global minimum at the low  $T$  is  $x = \mu_3$ , but there is a large energy barrier between  $x = \mu_2$  and  $x = \mu_3$  at low  $T$  so that the transition from  $x = \mu_2$  to  $x = \mu_3$  is unlikely. The shape of the potential for different temperatures is shown in Fig. 8(a). We design the triple-well potential to imitate the disordered state in the self-assemblies of DDQC by  $x = \mu_1$ , and the metastable state ( $\sigma \approx 0.6$ ) and the global minimum ( $\sigma \approx 0.8$ ) correspond to  $x = \mu_2$  and  $x = \mu_3$ , respectively.

We set  $\tau = 500$ ,  $dt = 1$ , and  $\xi_x$  following a normal distribution with mean zero and standard variation of 0.022. The parameters during the training of RL are chosen to be the same as the case for the DDQC formation given in Table 1, except that at each  $T$ , the number of update steps is set to 1000.

## 3 Results

### 3.1 Optimal temperature change to generate DDQC

First, we demonstrate the capability of Q-learning to find the best temperature schedule to create DDQCs of patchy particles from random configurations. Figure 4 shows the training result under the condition in Table 1, where the policy is trained with  $N_e = 101$  epochs and the initial temperature  $T_0$  at each epoch is randomly selected within the investigated range. At each epoch, the action changes according to the current policy and  $\epsilon$ , hence the states of temperature and  $\sigma$  change at each step, as shown in Fig. 4(a-b). At the first epoch in which  $\epsilon = 1$ , the action is random and  $T$  fluctuate around  $T \approx 1.0$ . Accordingly,  $\sigma$  is low  $\sigma < 0.2$  and far from the target value  $\sigma^*$ . As the training continues, Q-table is updated. At the mid epoch  $n = 51$  at which  $\epsilon = 0.5$ ,  $T$  fluctuates around  $T \approx 0.7$  whereas at the last epoch  $n = 101$  at which  $\epsilon = 0$ ,  $T$  shows less fluctuation around  $T \lesssim 0.7$ . After the epoch  $n = 51$ ,  $\sigma$  approaches closer to  $\sigma^*$ .

Figure 4(c) demonstrates the policy after training, which is the action for the maximum of  $Q$ , namely,  $\arg \max_a Q$ . This state-space roughly consists of two regions: decrease the temperature when  $T \gtrsim 0.7$ , and increase the temperature when  $T \lesssim 0.7$ . The action of "maintaining temperature" can be seen in the policy, but no clear correlation to the states is observed. The policy has states that are not accessed during training. The action for these inaccessible states is random. Figure 4(d) presents the ratio of the number of accessed states to total states during training (total number of states is  $10 \times 11$ ). We also measure whether the policy converges to its optimal in Fig. 4(e), by defining the ratio of the number of flipped states to accessed states. The flipped state is counted when the policy at the current epoch  $\pi^{(i)}(s, a)$  changes compared to the policy at the previous epoch  $\pi^{(i-1)}(s, a)$ . The ratio decays to  $\lesssim 0.1$ , but the decay is slow. Even after the epoch of  $\epsilon \lesssim 0.4$  after which the number of accessed states reaches a plateau, the ratio is still decaying slowly. This result suggests that many epochs are required to reach an optimal policy.

After training, the estimated policy is tested. The results of the test are presented in Fig. 5. The time evolution of temperature and  $\sigma$  during the test with initial configurations of random par-

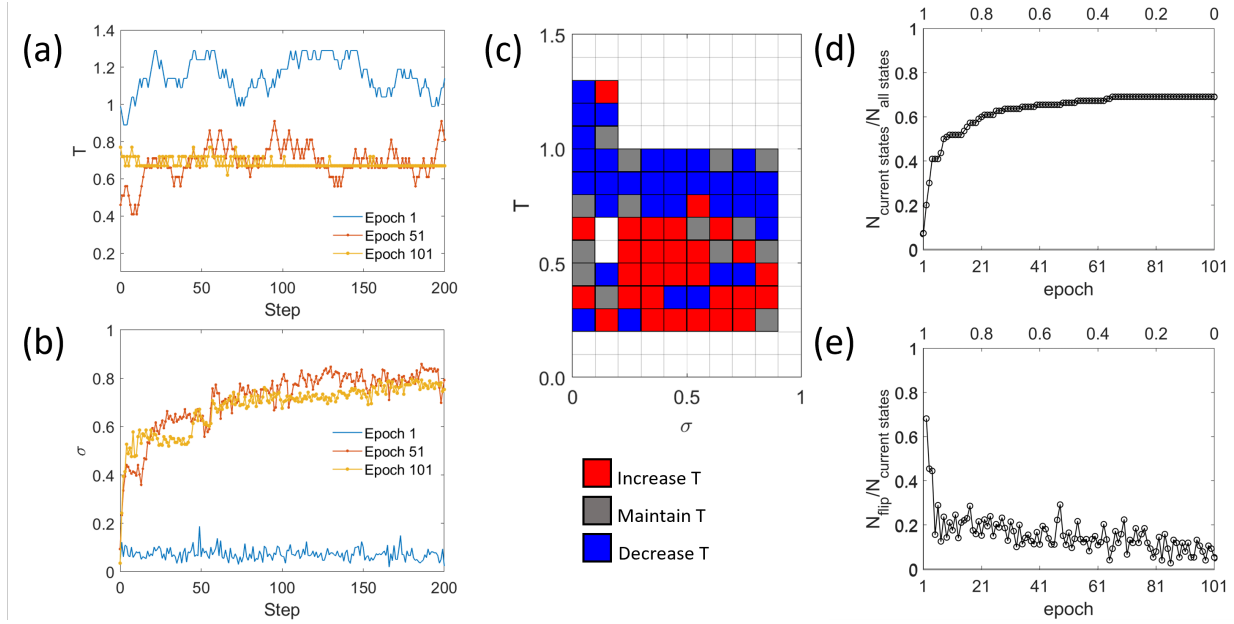


Fig. 4 Training data at the condition of random  $T_0$  and number of epochs  $N_e = 101$  in Table 1. (a,b) The progression of the states  $T$  and  $\sigma$  at selected epochs: first, middle and last epoch (equivalent  $\epsilon = 0, 0.5, 1$  respectively); (c) the policy after training; (d) the change of ratio of the number of accessed states to total states and (e) ratio of flipped-policy states to accessed states after each epoch during training, the horizontal axis on the top of the graph is the corresponding value of  $\epsilon$ .

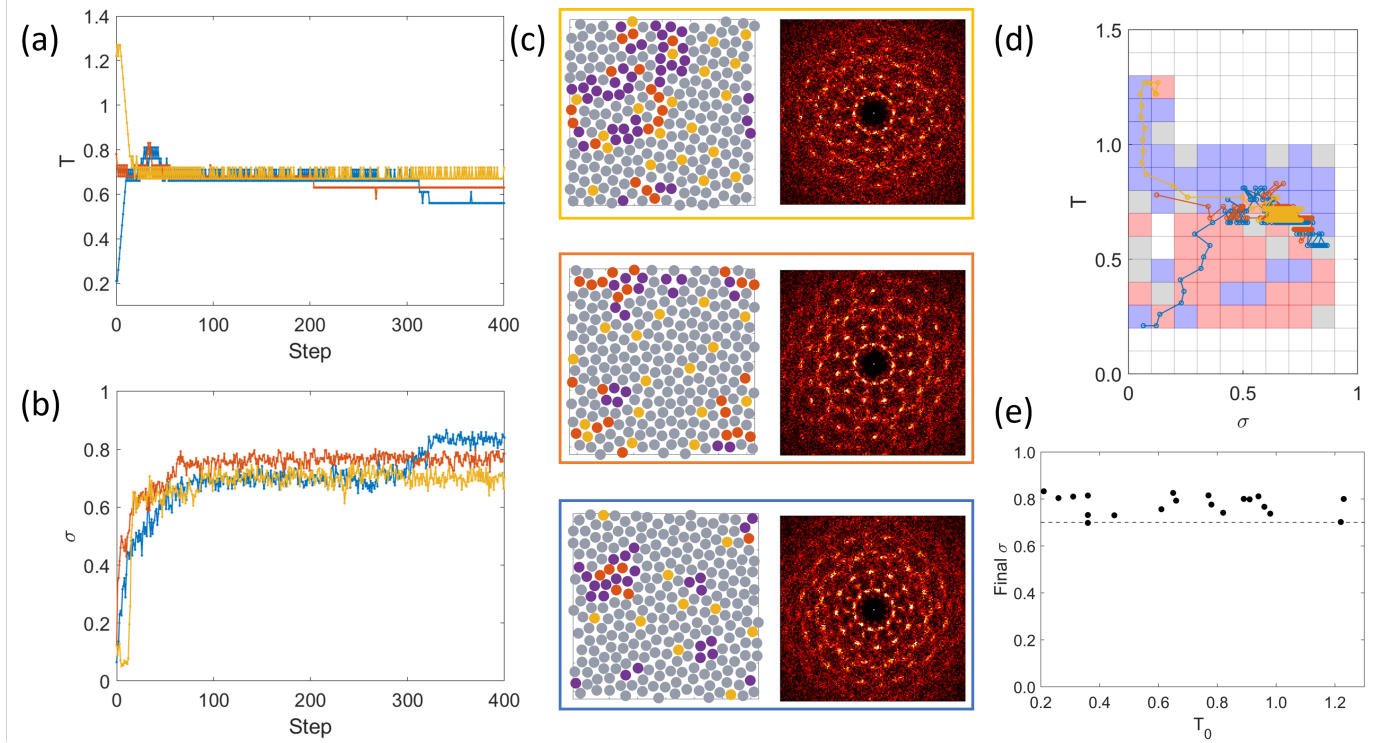


Fig. 5 Testing data of the policy obtained at the condition of random  $T_0$  and number of epochs  $N_e = 101$  in Fig. 4. (a) The temperature schedule, (b) its corresponding  $\sigma$ , and (c) snapshots at the last step of selected samples with the colours indicating the corresponding trajectories in (a) and (b). (d) The trajectories of (a,b) on the policy plane, in which the starting points are from the left side. (e) The dependence of  $\sigma$  on the initial temperature  $T_0$  obtained from 20 individual samples. The dashed line is a guide to the eye for the lower limit of global minimum DDQCs.

ticle positions and orientations and with random  $T_0$  are shown in Fig. 5(a,b). At first,  $T$  quickly reaches  $T \approx 0.7$ , then fluctuates around that value until  $\sigma$  reaches the target value. Finally,  $T$  decreases at a considerably slower rate to  $T \approx 0.6$ . The final temperature is dependent on each realisation; in some cases,  $T$  reaches  $T \approx 0.6$ , whereas, in other cases,  $T$  stays at  $T \approx 0.7$ . Correspondingly, the final value of  $\sigma$  is either  $\sigma \approx 0.8$  or slightly smaller than that. The snapshots at the final steps have dodecagonal motifs consisting of one  $Z$  particle centred in 18  $\sigma$  particles (see Fig.2(d)). The intensities in the Fourier space show clear twelve-fold symmetry, although some defects are present in the real space.

Figure 5(d) shows trajectories of the states ( $T$  and  $\sigma$ ) during the test together with the estimated policy. We show the three trajectories with different initial temperatures: high  $T_0$ , intermediate  $T_0$ , and low  $T_0$ . In the case of high  $T_0$ , the temperature decreases to  $T \approx 0.7$  but  $\sigma$  does not increase. Once the temperature becomes  $T \approx 0.7$ , dodecagonal structures start to appear and  $\sigma$  increases. Finally, the temperature decreases further to make  $\sigma$  larger.

In the case of low  $T_0$ , some dodecagonal structures appear from the beginning because the temperature is low. As the temperature is increased to  $T \approx 0.7$ ,  $\sigma$  is also increased and reaches  $\sigma \approx 0.7$ . The temperature is found to decrease at the point  $\sigma \approx 0.8$ .

When the initial temperature  $T_0$  is intermediate,  $\sigma$  is increased, then fluctuates, and finally, it is increased more when  $T_0$  is decreased slightly. Note that in all cases, the initial  $\sigma$  is small because the initial configuration of particles is random in position. Using this policy, the DDQC structure can be obtained in tests at any value of the initial temperature  $T_0$  (Fig. 5(e)).

Next, we compare the formation of a DDQC using the estimated policy with the self-assembly using the conventional annealing method.<sup>7</sup> Figure 6 shows the trajectories of  $T$  and  $\sigma$  for different realisations. In the case of the annealing, we have used the linear temperature decrease in BD steps. In this case, the time step for each BD step was also decreased for numerical stability. In both methods,  $\sigma$  values reach  $\sigma \approx 0.8$ , at which the dodecagonal structures appear clearly with a few defects. In the case of the annealing, we have used a pre-fixed temperature schedule, and therefore,  $t \gtrsim 2000$  is required for the dodecagonal structures. On the other hand, by using the estimated policy, we can get comparable structures in a much faster time. We should stress that when the slope of the temperature change is sharper for the pre-fixed schedule (which is referred to as quenching), the structure is trapped at the metastable state and the DDQC with few defects cannot be generated.<sup>7</sup>

We use a smaller system size,  $N = 256$ , in the training steps. It is important to check whether the estimated policy using RL can work upscale. We perform the test at larger system sizes  $N = 512$  and  $N = 1024$ . Figure 7 demonstrates the statistics of the obtained structure of different system sizes. The estimated policy for the smaller systems size works even for the tests with all investigated system sizes, namely, we obtain  $\sigma \gtrsim 0.7$ . The mean value of  $\sigma$  seems to slightly decrease with system size. This is because the larger system size requires more time to stabilise. If more steps are conducted for a larger system size, there is no significant dif-

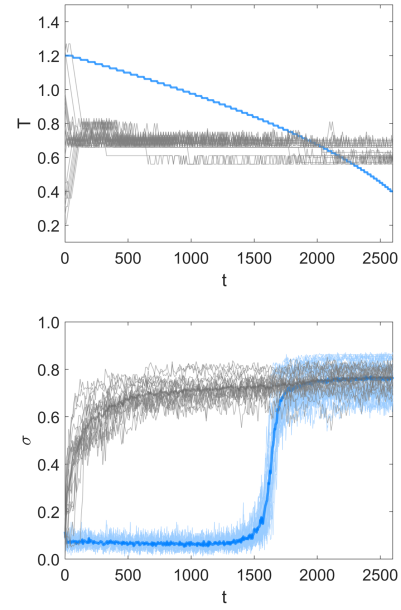


Fig. 6 Comparing DDQC assemblies by RL and annealing. The thin lines are the temporal changes of temperature and ratio of sigma of RL testing (grey) and annealing (blue) samples. The bold lines are the mean values of  $\sigma$ .

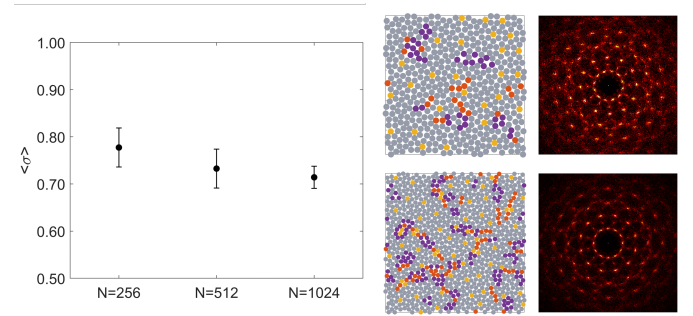


Fig. 7 Performance of the testing on different system sizes, where the policy is trained with the system of  $N = 256$  particles. The means and standard deviations are calculated from 20 independent samples. The snapshots and Fourier transformations are demonstrated for  $N = 512$  (upper) and  $N = 1024$  (lower) tests.

ference difference the three groups. In fact, the snapshots both in the real and Fourier spaces for the larger system sizes show dodecagonal structures.

### 3.2 Reinforcement learning for a simple model

To get a deeper insight into the mechanism of RL for DDQC formation, we apply Q-learning for a simple model. In this model, the state  $x$  (analogical to the state  $\sigma$  of DDQC) evolves under the triple-well potential shown in Fig. 8(a). We design the dependence of  $x$  on the temperature analogous to that of  $\sigma$  in DDQC. At high temperature, the local minimum is at  $x = 0.16$ , similar to the low  $\sigma$  structure. As the temperature decreases, this local minimum disappears, and two additional local minima appear at  $x = 0.55$  and  $x = 0.88$ . The former value imitates the metastable

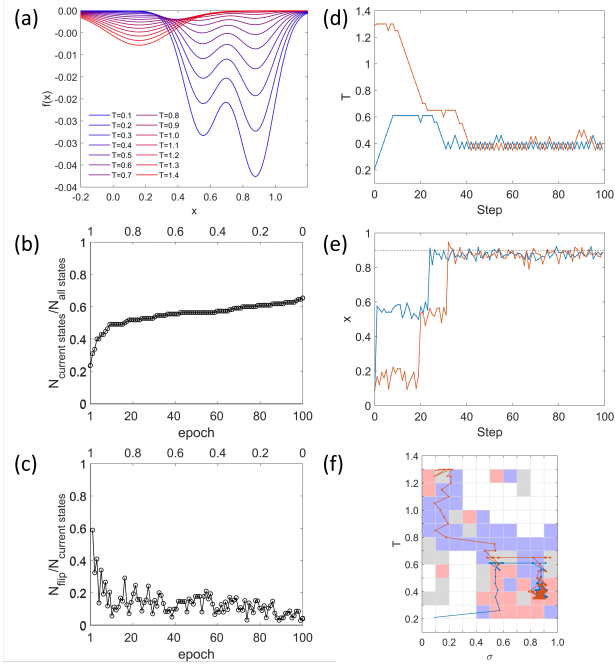


Fig. 8 Q-learning for the simple model trained with random  $T_0$  and number of epochs  $N_e = 100$ . (a) The triple-well potential. (b) The ratio of the number of accessed states to total states and (c) the ratio of flipped-policy states to accessed states during training. (d-e) The states  $T$  and  $x$  of two independent samples and (f) their trajectories on the policy plane, noting that the point size increases with the step.

state of a DDQC with many defects, whereas the latter corresponds to DDQC with fewer defects. By introducing the noise, a state  $x$  can jump from one well to the other well under intermediate temperature  $T$ .

The results of the training and testing are given in Fig. 8. We use the number of epochs  $N_e = 100$  and the random initial  $T = T_0$  at the beginning of each epoch. Figure 8(b,c) shows the ratio of the number of accessed states and the convergence of the policy during training of the Q-table. As the number of epochs increases (from  $\varepsilon = 1$  to  $\varepsilon = 0$ ), the number of accessed states increases, and the flip ratio converges slowly toward zero. Figure 8(d-f) depicts the time evolution of the states  $T$  and  $x$  of two testing samples and their trajectories on the policy plane. Starting with either a high or low value of  $T_0$ , the temperature quickly reaches  $T \approx 0.6$ , at which  $x$  fluctuates around the middle local minimum  $x = 0.55$ . After some time,  $T$  further decreases to a lower value  $T \approx 0.4$ , and accordingly,  $x$  goes to the deepest well. The estimated policy suggests two regions: decrease  $T$  when  $T > 0.6$  and increase  $T$  when  $T < 0.6$ . The boundary between the two regions is analogical to the critical temperature for the DDQC case.

## 4 Discussion and conclusion

Our results suggest that the best policy for making DDQC is to change the temperature quickly to the critical temperature  $T^* \approx 0.7$ , keep the temperature until the system is dominated by the dodecagonal structures, and then decrease the temperature further to the final temperature to get the structure with fewer defects. At the critical temperature, the structural fluctuations

are enhanced. As a result, there is more chance of getting the dodecagonal structure. At higher  $T$ , the particles are too mobile to make the ordered structures. On the other hand, at lower  $T$ , the particles are kinetically trapped in the metastable state, and it is unlikely to remove the defects. This temperature dependence is also seen in Fig. 6 and Fig. 9 in Ref.<sup>7</sup> about the formation of DDQC under the annealing (slow temperature change) and quenching (rapid temperature change). From the initial condition of random positions and orientations, the patchy particles cannot form DDQC by rapid quenching because the system gets trapped in the metastable state. In the estimated policy by RL, even when we start from low  $T_0$ , the policy suggests increasing temperature so that the system may escape from the metastable state. In<sup>7</sup>, the DDQC can be generated by fixed annealing, which is sufficiently slow. However, this fixed temperature schedule is not efficient because it takes too much time to reach the critical temperature at which structural transition occurs. RL can learn that the critical temperature  $T^*$  plays an important role in enhancing the probability of QC structural formation. We stress that our method feeds neither existence of the critical temperature nor its value. Our RL method automatically finds them during the training steps.

As shown in Fig 4, the convergence to reach the steady state of the iteration for optimising the policy is very slow. Therefore, many epochs are required. Here, we discuss whether we may reduce the computational/training cost using prior knowledge. During training, instead of using random initial temperature  $T_0$  for each epoch, we consider the situation of fixed  $T_0$  either at high or low temperature. We also vary the number of epochs for each training set. The policies of those training sets are then evaluated. Figure 9 presents the  $\sigma$  of the testing samples for many training sets. It is noted that regardless of the condition of  $T_0$  during training, we use the random  $T_0$ . In general, the more number of epochs used during training, the better the policy is; namely, more structures with  $\sigma > 0.7$  can be obtained during the test. More importantly, the value of  $T_0$  during training affects the performance of the policy. For example, even when the number of epochs is  $N_e = 20$ , the policy of ‘low  $T_0$ ’ training set works well for the test with low  $T_0$  but fails for the test with high  $T_0$ . On the other hand, the policy trained by the ‘high  $T_0$ ’ training set works well for the test with high  $T_0$  but fails for the test with low  $T_0$ . In other words, if we have a constraint of the initial temperature  $T_0$  in the system, we may reduce the computational cost. This is because the search space during training is smaller. The drawback of the constraint is that the trained policy cannot work outside the constraint.

The choice of statistical quantities that characterise the structures is crucial for designing a successful RL system. This includes the choice of the relevant states and how finely to discretise the states (for Q-table). In the case of DDQC, the continuous state we choose is the ratio of the  $\sigma$  particles because  $\sigma$  can span over a wide range in  $[0, 1]$ , therefore the DDQC structures can be distinguished more easily. One can consider the  $Z$  particles to evaluate the DDQC structure. However, under the same condition, the performance of Q-learning with  $Z$  is not as good as Q-learning with  $\sigma$  because the ratio of  $Z$  spans over a more narrow range.

In this work, we use the Q-table to perform the Q-learning. The

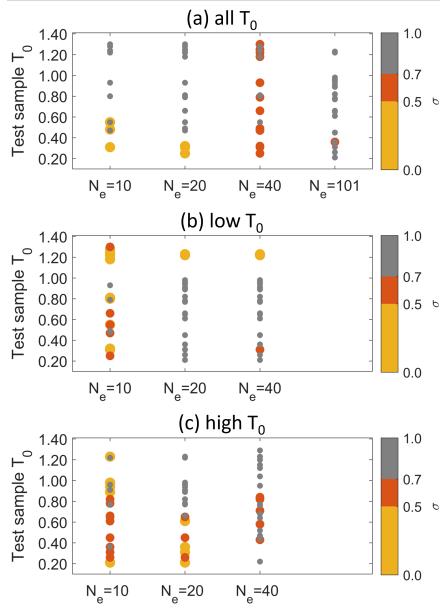


Fig. 9 Performance of RL tests at different training sets at the condition (a) all  $T_0$ , (b) low  $T_0$  and (c) high  $T_0$  in Table 2. The horizontal axis labels indicate the number of epochs  $N_e$  during training. The vertical axes indicate the initial temperature  $T_0$  during the tests. The colours of the spots indicate  $\sigma$  values during the tests. The size of the point is for better visualisation.

DDQC self-assembly has the continuous states  $\sigma$  and  $T$  whose essential features can be captured even after discretisation. In this case, the method of Q-table works and is easily implemented. However, the drawback is that the policy is sensitive to such discreteness, as it can not distinguish between the adjacent states and as a result, the agent is trapped in a state-action space and not able to find a better solution. For example, some testing samples trapped in the metastable states can escape from the metastable states and become DDQC, while others cannot escape. In order to avoid such local traps, one may consider a non-zero epsilon value (finite amplitude of noise) during the tests. Figure 10 shows the effect of adding noise on the tests. Figure 10(a-c) illustrates the time evolution of  $T$  and  $\sigma$  of two tests with  $\epsilon = 0$  and  $\epsilon = 0.2$ . In the former case, the temperature change strictly follows the policy, while it has some noises or randomness in the latter case. Adding noise can help the testing sample escape the metastable state and become DDQC in this sample. However,  $\epsilon = 0.2$  does not always result in DDQC and statistically the test results are not improved by the noise (Fig. 10(d)). Therefore, in the current setting, discretisation of the state space does not seem to have serious effects on the estimated policy.

When the dimension of states is much higher, Q-table is not manageable. Approximation of the Q-function by the small number of continuous basis functions is promising in this direction.

So far in this study, the policy is trained with the  $\epsilon$ -greedy approach. The choice of the action is dependent on the current  $\epsilon$  and the Q-table. Here we discuss that the RL also works even when the training is off-policy, i.e. during training, the actions at every step are randomly chosen from the action space ( $\epsilon = 1$ ). Figure 11 displays the values of  $T$  and  $\sigma$  during training, and

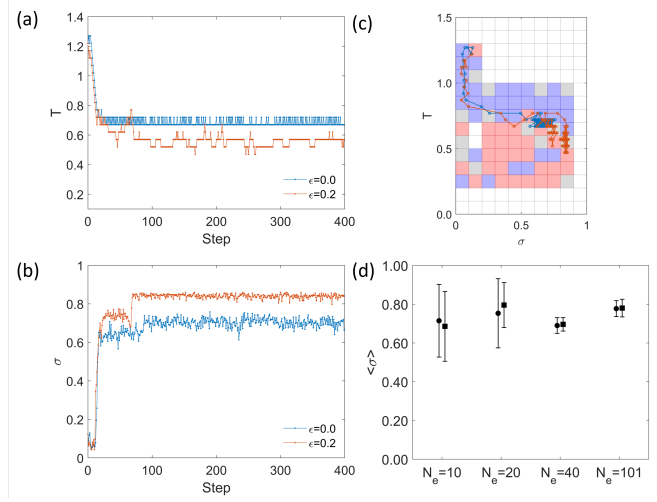


Fig. 10 The effect of adding noise on testing. (a,b) Progress of  $T$  and  $\sigma$  at  $\epsilon = 0$  and  $\epsilon = 0.2$  of selected samples for the policy obtained in Table 1 and (c) corresponding trajectories in the policy plane; (d) Error bar graph showing the effect of adding noise on the performance of the testing for different training data sets (parameters are given in Table 1) with  $\epsilon = 0.0$  (filled circles) and  $\epsilon = 0.2$  (filled squares).

the trajectories of two independent tests on the policy plane. Two regions, decreasing temperature and increasing temperature, can be seen on the policy plane. The test with high  $T_0$  follows the policy, that is to decrease  $T$  to the critical temperature  $T^*$ , and stay there so that the DDQC structure is formed. The test with low  $T_0$  starts at the inaccessible states. Therefore, the action applied to the temperature is random until the trajectory hits the accessed states. Then, the trajectory follows the estimated policy and eventually DDQC structure is observed. We can see that the number of accessed states in Fig. 11(b) is less than the one in Fig. 4. This indicates that the transition probability between the accessed states is higher, and policy at the accessed states is well trained. The non-accessed states in Fig. 11(b), for example, the states at the low left corner, have random policies. In our system, these policies work because, after random fluctuations of temperature, the trajectory hits the region of  $T < 0.5$  and  $\sigma > 0.4$  in the policy in Fig. 11(b) and then it goes to the critical temperature. Then, the structure becomes DDQC. For this reason, the completely off-policy training works in our system. Still, we suspect it does not work for other systems.

To summarise, we propose the method based on RL to estimate the best policy of temperature control for the self-assemblies of patchy particles to obtain the DDQC structures. From the estimated policy, we successfully obtain the DDQCs even for the system size larger than the size we use for training. The key to the success is that RL finds the critical temperature of the DDQC self-assembly during training. The estimated policy suggests that first, we change the temperature to the critical temperature so that the larger fluctuations enhance the probability of forming DDQC, and then decrease the temperature slightly to remove defects. The estimated policy is more efficient than the pre-fixed temperature schedule used in the previous studies and DDQC can be generated in a shorter time. The mechanism of learning op-



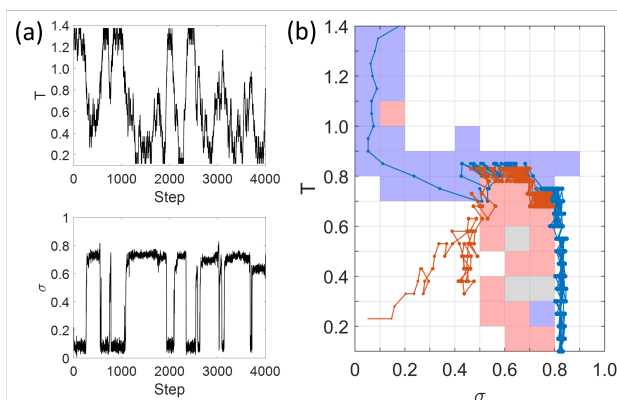


Fig. 11 Off-policy training for DDQC. (a) The states  $T$  and  $\sigma$  during training. (b) Policy and the behaviour of testing samples at different  $T_0$  on the policy plane.

timal policy is demonstrated in the simple triple-well model. In order to avoid metastable states, the optimal policy suggests increasing the temperature if we start from a low temperature. We believe that the method presented in this work can be applied to other self-assembly problems.

## Author Contributions

U.L. performed the simulations and analysed the data. N.Y. designed the research. All the authors developed the method and were involved in the evaluation of the data and the preparation of the manuscript.

## Conflicts of interest

There are no conflicts to declare.

## Acknowledgements

The authors acknowledge the support from JSPS KAKENHI Grant number JP20K14437, JP23K13078 to U.T.L., and JP20K03874 to N.Y. This work is support also by JST FOREST Program Grant Number JPMJFR2140 to N.Y.

## Notes and references

- 1 A.-P. Hynninen, J. H. J. Thijssen, E. C. M. Vermolen, M. Dijkstra and A. van Blaaderen, *Nature Materials*, 2007, **6**, 202–205.
- 2 M. He, J. P. Gales, É. Ducrot, Z. Gong, G.-R. Yi, S. Sacanna and D. J. Pine, *Nature*, 2020, **585**, 524–529.
- 3 R. Tamura, A. Ishikawa, S. Suzuki, T. Kotajima, Y. Tanaka, T. Seki, N. Shibata, T. Yamada, T. Fujii, C.-W. Wang, M. Avdeev, K. Nawa, D. Okuyama and T. J. Sato, *Journal of the American Chemical Society*, 2021, **143**, 19938–19944.
- 4 K. Deguchi, S. Matsukawa, N. K. Sato, T. Hattori, K. Ishida, H. Takakura and T. Ishimasa, *Nature materials*, 2012, **11**, 1013–1016.
- 5 Q. Chen, S. C. Bae and S. Granick, *Nature*, 2011, **469**, 381–384.
- 6 I. E. Ventura Rosales, L. Rovigatti, E. Bianchi, C. N. Likos and E. Locatelli, *Nanoscale*, 2020, **12**, 21188–21197.
- 7 U. T. Lieu and N. Yoshinaga, *Soft Matter*, 2022, **18**, 7497–7509.
- 8 S. C. Glotzer and M. J. Solomon, *Nat Mater*, 2007, **6**, 557–562.
- 9 M. Engel, P. F. Damasceno, C. L. Phillips and S. C. Glotzer, *Nat Mater*, 2015, **14**, 109–116.
- 10 Y. Geng, G. Van Anders and S. C. Glotzer, *Nanoscale*, 2021, **13**, 13301–13309.
- 11 R. Kumar, G. M. Coli, M. Dijkstra and S. Sastry, *The Journal of Chemical Physics*, 2019, **151**, 084109.
- 12 Y. Ma and A. L. Ferguson, *Soft Matter*, 2019, **15**, 8808–8826.
- 13 U. T. Lieu and N. Yoshinaga, *The Journal of Chemical Physics*, 2022, **156**, 054901.
- 14 N. Yoshinaga and S. Tokuda, *Phys. Rev. E*, 2022, **106**, 065301.
- 15 M. N. van der Linden, J. P. K. Doye and A. A. Louis, *The Journal of Chemical Physics*, 2012, **136**, 054904.
- 16 J. Bechhoefer, *Control theory for physicists*, Cambridge University Press, 2021.
- 17 D. Silver, T. Hubert, J. Schrittwieser, I. Antonoglou, M. Lai, A. Guez, M. Lanctot, L. Sifre, D. Kumaran, T. Graepel, T. Lillicrap, K. Simonyan and D. Hassabis, *Science*, 2018, **362**, 1140–1144.
- 18 OpenAI Five Defeats Dota 2 World Champions, <https://openai.com/research/openai-five-defeats-dota-2-world-champions>.
- 19 T. Zhang and H. Mo, *International Journal of Advanced Robotic Systems*, 2021, **18**, 172988142110073.
- 20 S. Verma, G. Novati and P. Koumoutsakos, *Proceedings of the National Academy of Sciences*, 2018, **115**, 5849–5854.
- 21 P. Garnier, J. Viquerat, J. Rabault, A. Larcher, A. Kuhnle and E. Hachem, *Computers & Fluids*, 2021, **225**, 104973.
- 22 M. Nasiri and B. Liebchen, *New Journal of Physics*, 2022, **24**, 073042.
- 23 Z. Huang, X. Liu and J. Zang, *Nanoscale*, 2019, **11**, 21748–21758.
- 24 J. Zhang, J. Yang, Y. Zhang and M. A. Bevan, *Science Advances*, 2020, **6**, eabd6716.
- 25 M. M. Norton, P. Grover, M. F. Hagan and S. Fraden, *Phys. Rev. Lett.*, 2020, **125**, 178005.
- 26 M. J. Falk, V. Alizadehyazdi, H. Jaeger and A. Murugan, *Phys. Rev. Res.*, 2021, **3**, 033291.
- 27 M. Durve, F. Peruani and A. Celani, *Phys. Rev. E*, 2020, **102**, 012601.
- 28 S. Whitelam and I. Tamblin, *Phys. Rev. E*, 2020, **101**, 052604.
- 29 Q. Wei, F. L. Lewis, Q. Sun, P. Yan and R. Song, *IEEE Transactions on Cybernetics*, 2017, **47**, 1224–1237.
- 30 R. A. DeLaCruz-Araujo, D. J. Beltran-Villegas, R. G. Larson and U. M. Córdoba-Figueroa, *Soft Matter*, 2016, **12**, 4071–4081.
- 31 S. L. Brunton and J. N. Kutz, *Data-Driven Science and Engineering: Machine Learning, Dynamical Systems, and Control*, Cambridge University Press, 2nd edn, 2022.
- 32 R. S. Sutton and A. G. Barto, *Reinforcement Learning: An Introduction*, MIT Press, Cambridge, Mass, 1998.